RESEARCH ARTICLE





Formation and hydrolysis of gas-phase $[UO_2(R)]^+$: R=CH₃, CH₂CH₃, CH=CH₂, and C₆H₅

Irena Tatosian¹ | Amanda Bubas^{1,2} | Anna Iacovino¹ | Susan Kline¹ | Luke Metzler¹ | Michael Van Stipdonk¹

Correspondence

Michael Van Stipdonk, Department of Chemistry and Biochemistry, Duquesne University, 600 Forbes Ave, Pittsburgh, PA 15282, USA.

Email: vanstipdonkm@duq.edu

Funding information

National Science Foundation, Grant/Award Numbers: CHE-1659823, CHE-1726824 and CHE-0963450; Duquesne University; BSNES

Abstract

The goals of the present study were (a) to create positively charged organo-uranyl complexes with general formula $[UO_2(R)]^+$ (eg, R=CH₃ and CH₂CH₃) by decarboxylation of [UO₂(O₂C-R)]⁺ precursors and (b) to identify the pathways by which the complexes, if formed, dissociate by collisional activation or otherwise react when exposed to gas-phase H₂O. Collision-induced dissociation (CID) of both [UO₂(O₂C—CH₃)]⁺ and [UO₂(O₂C—CH₂CH₃)]⁺ causes H⁺ transfer and elimination of a ketene to leave [UO₂(OH)]⁺. However, CID of the alkoxides [UO₂(OCH₂CH₃)]⁺ and [UO₂(OCH₂CH₃)]⁺ produced [UO₂(CH₃)]⁺ and [UO₂(CH₂CH₃)]⁺, respectively. Isolation of [UO₂(CH₃)]⁺ and [UO₂(CH₂CH₃)]⁺ for reaction with H₂O caused formation of $[UO_2(H_2O)]^+$ by elimination of $\cdot CH_3$ and $\cdot CH_2CH_3$: Hydrolysis was not observed. CID of the acrylate and benzoate versions of the complexes, $[UO_2(O_2C-CH=CH_2)]^+$ and $[UO_2(O_2C-C_6H_5)]^+$, caused decarboxylation to leave $[UO_2(CH=CH_2)]^+$ and $[UO_2(C_6H_5)]^+$, respectively. These organometallic species do react with H₂O to produce [UO₂(OH)]⁺, and loss of the respective radicals to leave [UO₂(H₂O)]⁺ was not detected. Density functional theory calculations suggest that formation of $[UO_2(OH)]^+$, rather than the hydrated $U^VO_2^+$, cation is energetically favored regardless of the precursor ion. However, for the [UO₂(CH₃)]⁺ and [UO₂(CH₂CH₃)]⁺ precursors, the transition state energy for proton transfer to generate $[UO_2(OH)]^+$ and the associated neutral alkanes is higher than the path involving direct elimination of the organic neutral to form [UO₂(H₂O)]⁺. The situation is reversed for the $[UO_2(CH=CH_2)]^+$ and $[UO_2(C_6H_5)]^+$ precursors: The transition state for proton transfer is lower than the energy required for creation of [UO₂(H₂O)]⁺ by elimination of CH=CH₂ or C₆H₅ radical.

KEYWORDS

 $collision-induced\ dissociation,\ electrospray\ ionization,\ organometallic,\ tandem\ mass\ spectrometry,\ uranyl\ ion$

1 | INTRODUCTION

Recent experiments by our group have demonstrated that lower levels of adventitious H_2O in a linear ion trap (LIT) mass spectrometer can provide access to fragmentation pathways and reactions for gas-phase

uranyl ($U^{VI}O_2^{2+}$) complexes that were not observed during previous experiments conducted with a three-dimensional quadrupole ion trap (QIT).¹⁻⁷ When H₂O levels in an ion trap are high, precursor complexes that are isolated for collision-induced dissociation (CID) tend to undergo association reactions to make adducts or charge reduction

780 © 2019 John Wiley & Sons, Ltd. wileyonlinelibrary.com/journal/jms JMassSpectrom . 2019;**54**:780–789.

¹Department of Chemistry and Biochemistry, Duquesne University, 600 Forbes Ave, Pittsburgh, Pennsylvania 15282, USA

² Department of Chemistry, University of Utah, 215 1400 E, Salt Lake City, UT 84112

reactions to form products such as $[UO_2(OH)]^+$, $[UO_2]^+$, and hydrates of these cations.8-12 For example, with complexes of UO22+ coordinated by acetone, the H₂O addition rates were so fast that fragment ions containing two or three acetone ligands, generated by CID of larger precursors, hydrated to generate heterogeneous, tetra-, or penta-coordinate complexes that dominated the product ion spectrum. ⁹ This prevented the detailed investigation of complex ions containing UO22+ and two or fewer ligands. However, in a recent investigation of the fragmentation behavior of UO22+ complexes containing acetonitrile, we demonstrated that the lower levels of background H₂O in a LIT allowed us to produce bare UO₂²⁺ by multiplestage CID and generate an [NUO]⁺ product by CID of [UO₂(NC)]⁺. While gas-phase [NUO]⁺ had been created by Heinemann and Schwarz using insertion of U+ into NO in an ion-molecule reaction (IMR).¹³ our experiments demonstrated that the species can also be produced in a CID reaction through a (putative) cyanate intermediate.

The low level of background H_2O in the LIT also allowed us to revise the intrinsic dissociation pathways for a range of species such as $[UO_2(NO_3)]^+$, $[UO_2(CIO_4)]^+$, and $[UO_2(O_2C-CH_3)_3]^{-}$.^{3,6,7} For example, with relatively high levels of background H_2O , CID of $[UO_2(NO_3)]^+$ generated peaks corresponding to $[UO_2(H_2O)]^+$ and UO_2^+ . However, with lower levels of background H_2O , the dominant product ion generated by CID of $[UO_2(NO_3)]^+$ was $[UO_2(O_2)]^+$, created by the ejection of NO. When isolated for IMR, the $[UO_2(O_2)]^+$ product can undergo a facile exchange reaction with H_2O to leave $[UO_2(H_2O)]^+$, thus explaining the observations made when using an ion trap with high levels of background H_2O .

In another set of experiments that are relevant to the present study, electrospray ionization (ESI) and multiple-stage (MSn) tandem mass spectrometry were used to create and characterize ions derived from anionic UO22+-formate and -acetate precursors.3 When the levels of background H₂O are low, [UO₂(O₂C-H)₃]⁻ fragments by decarboxylation and elimination of CH2=O, ultimately to produce the oxo-hydride [UO2(O)(H)]. The primary fragmentation pathway for [UO₂(O₂C-CH₃)₃]⁻ is elimination of acetyloxyl radical, CH₃CO₂. with reduction of UO22+ to UO2+. Subsequent CID of [UO₂(O₂C-CH₃)₂] formed the organometallic complex [UO₂(CH₃) (O₂C-CH₃)] by decarboxylation. The organometallic product then reacted with H₂O to produce [UO₂(OH)(O₂C-CH₃)]⁻ (and neutral CH₄) when independently isolated for IMR with H₂O. CID of the [UO₂(CH₃)(O₂C-CH₃)] species caused intracomplex proton transfer and loss of CH₄ to create [UO₂(O₂C=CH₂)]⁻, which subsequently fragmented to generate [UO2(O)]-. These reaction pathways were in contrast to an earlier report by Luo et al, 14 who listed species such as [UO₂(CH₃)(OH)]⁻ and [UO₂(OH)₂]⁻ among terminal dissociation products. Our experiments demonstrated that the ions are instead artifacts of reactions between CID products and background H2O.

Our experiments with formate and acetate complexes followed a previous study ¹⁵ in which a QIT was used to investigate the dissociation reactions of anionic actinyl complexes with carboxylate ligands. Precursor ions with the general formula $[AnO_2(O_2C-R)_3]^-$, where An = U, Np, and Pu and R = CH₃ (methyl), CH₃C \equiv C (1-propynyl), C₆H₅ (phenyl), and C₆F₅ (pentafluorophenyl), were subjected to CID.

Product ions such as $[(R)AnO_2(O_2C-R)_2]^-$ and $[(R)_2AnO_2(O_2C-R)]^-$ were generated by decarboxylation, and this was the first report of such species that included discrete Np—C and Pu—C bonds.

Given the interesting actinyl complexes generated in the negative ion mode, the goals of the present study were (a) to determine whether similar, cationic uranyl-alkyl or aryl complexes with general formula $[UO_2(R)]^+$ could be produced by decarboxylation of $[UO_2(O_2C-R)]^+$ precursors and (b) to identify the pathways by which the species, if formed, dissociate by collisional activation or otherwise react when exposed to gas-phase H_2O . Our hypothesis was that lower levels of adventitious H_2O would improve the likelihood that the organometallic species would be generated by multiple-stage CID.

2 | EXPERIMENTAL METHODS

2.1 | Sample preparation

Ethanol (CH₃CH₂OH) and 1-propanol (CH₃CH₂CH₂OH) were purchased from Sigma-Aldrich Chemical (St. Louis, MO) and used as received. Samples necessary to prepare gas-phase uranyl-acetate, propionate, -acrylate, or -benzoate cations were prepared by combining 2 to 3 mg of UVIO3 (Strem Chemicals, Newburyport, MA), corresponding to approximately 7×10^{-6} to 1×10^{-5} moles, with a twofold mole excess of the respective carboxylic acids (Sigma Aldrich, St. Louis, MO) and 400 µL of deionized/distilled H₂O in a glass scintillation vial. The solutions were allowed to incubate on a hot plate at 70°C for 12 hours. Caution: uranium oxide is radioactive (α - and γ -emitter), and proper shielding, waste disposal, and personal protective gear should be used when handling the material. When cooled, 20 µL of the resulting solution was diluted with 800 µL of 50:50 (by volume) H₂O:CH₃CH₂OH and used without further work up as the spray solution for ESI-MS. CH₃CH₂OH is used as co-solvent in most of our experiments to avoid any ambiguity when looking for potential molecular O₂ adducts to product ions. 16-19 With the limited mass measurement accuracy of the LIT, O2 and CH3OH adducts cannot be distinguished. As discussed below, CH₃CH₂CH₂OH was used for one set of experiments to generate the [UO2(CH2CH3)]+ precursor for investigation of reaction with H2O.

ESI and CID experiments were performed on a ThermoScientific (San Jose, CA) LTQ-XL LIT mass spectrometer. The spray solutions were infused into the ESI-MS instrument using the incorporated syringe pump at a flow rate of 5 μ L/min. In the positive ion mode, the atmospheric pressure ionization stack settings for the LTQ (lens voltages, quadrupole and octopole voltage offsets, etc) were optimized for maximum transmission of singly charged ions such as $[UO_2(O_2C-R)(CH_3CH_2OH)_2]^+$ and $[UO_2(O_2C-R)(CH_3CH_2OH)_3]^+$ to the LIT by using the auto-tune routine within the LTQ Tune program. Helium was used as the bath/buffer gas to improve trapping efficiency and as the collision gas for CID experiments.

For CID, precursor ions were isolated using a width of 1.0 to 1.5 m/z units. The exact value was determined empirically to provide maximum ion intensity while ensuring isolation of a single isotopic peak.

To probe CID behavior in general, the (mass) normalized collision energy (NCE, as defined by ThermoScientific) was set between 5% and 18%, which corresponds to 0.075 to 0.27 V applied for CID with the current instrument calibration. The activation Q, which defines the frequency of the applied radio frequency potential, was set at 0.30, and a 30-ms activation time was used.

To probe gas-phase reactions of selected precursor ions with background neutrals, ions were isolated using widths of 1 to 2 m/z units. Here too, the specific width used was chosen empirically to ensure maximum ion isolation efficiency. The ions were then stored in the LIT for periods ranging from 1 ms to 10 s. Despite the lower H₂O levels in the 2-D LIT under normal operating conditions, there is still a sufficient partial pressure of the neutral to permit an investigation of IMRs, particularly when using long isolation times. Our intent was not to measure or report rates or rate constants but to identify the pathways by which ions react with neutrals such as H2O or O2 in the LIT. The levels of these neutral species in the LIT are too low to allow a rigorous examination of H₂O addition rates to specific uranyl complexes for comparison to earlier studies, and our instrument is not configured to allow controlled addition of neutral reagents for IMR. For both CID and IMR experiments, the mass spectra displayed were created by accumulating and averaging at least 30 isolation, dissociation, and ejection/detection steps.

2.2 | DFT calculations

Geometry optimizations for potential product ion structures were performed using the B3LYP, ²⁰⁻²² PBEO, ^{23,24} M06-L and M06-2X functionals, ²⁵ the MWB60 pseudopotential and associated basis set on U, and the 6-311 + G(d,p) basis set on all other atoms. In all cases, an ultrafine integration grid was used. Vibrational frequency calculations were used to determine whether optimized structures were true minima (no imaginary frequencies) or transition states (one imaginary frequency) and for zero-point and thermal correction of energies. Transition state calculations for the hydrolysis of organometallic complexes were performed using the QST2 and QST3 methods. ²⁶ Intrinsic reaction coordinate (IRC) calculations were used to confirm that the transition states bridged the appropriate minima. The Gaussian 16 software package ²⁷ was used for all calculations.

3 | RESULTS AND DISCUSSION

3.1 | Creation of $[UO_2(R)]^+$ species and reactions with gas-phase H_2O

As noted earlier, one aim of this study was to create cationic uranylalkyl and -aryl complexes by decarboxylation using MSⁿ CID. This approach has been used extensively to create a range of organometallic species, including some that contain ${\rm UO_2}^{2^+}$, for gas-phase studies. $^{3,15,28-31}$ In several cases, the positively and negatively charged organometallic species were created for subsequent study of hydrolysis in a species-specific fashion. 3,15,28,29,31

The MSⁿ CID of $[UO_2(O_2C-CH_3)(CH_3CH_2OH)_n]^+$, n = 0 - 3, was discussed in our previous report.3 For the sake of comparison with the respective carboxylate precursors presented below, the MSⁿ spectra are provided in Figure S1 and briefly summarized here. The most abundant positively charged species generated by ESI of uranyl acetate in 50:50 H₂O/CH₃CH₂OH was [UO₂(O₂C-CH₃)(CH₃CH₂OH)₂]⁺ at m/z 421 (Figure S1A). CID of $[UO_2(O_2C-CH_3)(CH_3CH_2OH)_2]^+$ caused elimination of single CH₃CH₂OH ligands in sequential stages (MS/MS and MS³ stages, Figure S1B,C, respectively) to generate $[UO_2(O_2C-CH_3)]^+$ at m/z 329. Subsequent CID (Figure S1D) of $[UO_2(O_2C-CH_3)]^+$ generated $[UO_2(OH)]^+$ at m/z 287. The product ion shifted to m/z 288 for CID of [UO₂(O₂C-CD₃)]^{+,3} consistent with a dissociation reaction pathway that involves intramolecular H⁺(D⁺) transfer and elimination of ketene O=C=CH₂ (O=C=CD₂ for the deuterium labeled analog) as suggested by Waters et al.³² Formation of $[UO_2(CH_3)]^+$ by decarboxylation of $[UO_2(O_2C-CH_3)]^+$ did not occur.

Graul and Squires used CID of (bare) ethoxide to synthesize the methyl carbanion for studies of gas-phase reactivity in a flowing afterglow instrument. We found that sufficient abundance of ethanol-coordinated uranyl-ethoxide cation, $[UO_2(OCH_2CH_3)(CH_3CH_2OH)_2]^+$, was created by ESI of the uranyl-acetate solution (in 50:50 H₂O: CH₃CH₂OH) to allow preparation of $[UO_2(OCH_2CH_3)]^+$ by MSⁿ CID. Subsequent CID of $[UO_2(OCH_2CH_3)]^+$ created $[UO_2(CH_3)]^+$.

The CID of $[UO_2(CH_3)]^+$ was probed in our previous study³; the sole fragmentation pathway is creation of $[UO_2]^+$ (m/z 270) by elimination of CH₃ radical. The product ion spectra generated by isolation of $[UO_2(CH_3)]^+$ at m/z 285, without imposed collisional excitation, for reaction with background neutrals (presumed to be primarily H₂O and O₂) over time periods ranging from 1 ms to 1 s are shown in Figure 1. At isolation times of 10 and 100 ms, (Figure 1A,B, respectively), $[UO_2(H_2O)]^+$ and UO_2^+ product ions at m/z 288 and 270, respectively, were observed. At isolation times of 1 and 10 s (Figure 1C,D, respectively), larger hydrates such as $[UO_2(H_2O)_2]^+$ and $[UO_2(H_2O)_3]^+$ at m/z 306 and 324, along with the O₂ adduct $[UO_2(H_2O)(O_2)]^+$, ¹⁶⁻¹⁸ are also formed.

The appearance of the $[UO_2(H_2O)]^+$ is likely the result of reaction 1, in which the energy associated with binding of H_2O drives the elimination of $\cdot CH_3$ and reduction of uranyl to $UO_2^{2^+}$. The formation of UO_2^{+} may involve either collisions with He or H_2O with sufficient energy to cause reductive elimination of $\cdot CH_3$ directly or the loss of H_2O from the $[UO_2(H_2O)]^+$ product created in reaction 1.

$$\begin{split} &[\mathsf{UO}_2(\mathsf{CH}_3)]^+ + \mathsf{H}_2\mathsf{O} {\to} [\mathsf{UO}_2(\mathsf{CH}_3)(\mathsf{H}_2\mathsf{O})]^{+*} {\to} [\mathsf{UO}_2(\mathsf{H}_2\mathsf{O})]^+ \\ &+ \cdot \mathsf{CH}_3. \end{split} \tag{1}$$

While a hydrolysis pathway was observed for anionic actinyl organometallic complexes in earlier studies, 3,15 the formation of $[UO_2(OH)]^+$ (m/z 287) and elimination of CH_4 (reaction 2) was not detected above background in the present study (Figure 1).

$$\begin{array}{l} [\mathsf{UO}_2(\mathsf{CH}_3)]^+ \\ + \mathsf{H}_2\mathsf{O} \!\!\to\!\! [\mathsf{UO}_2(\mathsf{CH}_3)(\mathsf{H}_2\mathsf{O})]^{+*} \!\!\to\!\! [\mathsf{UO}_2(\mathsf{OH})(\mathsf{CH}_4)]^{+*} \!\!\to\!\! [\mathsf{UO}_2(\mathsf{OH})]^+ \\ + \mathsf{CH}_4. \end{array}$$

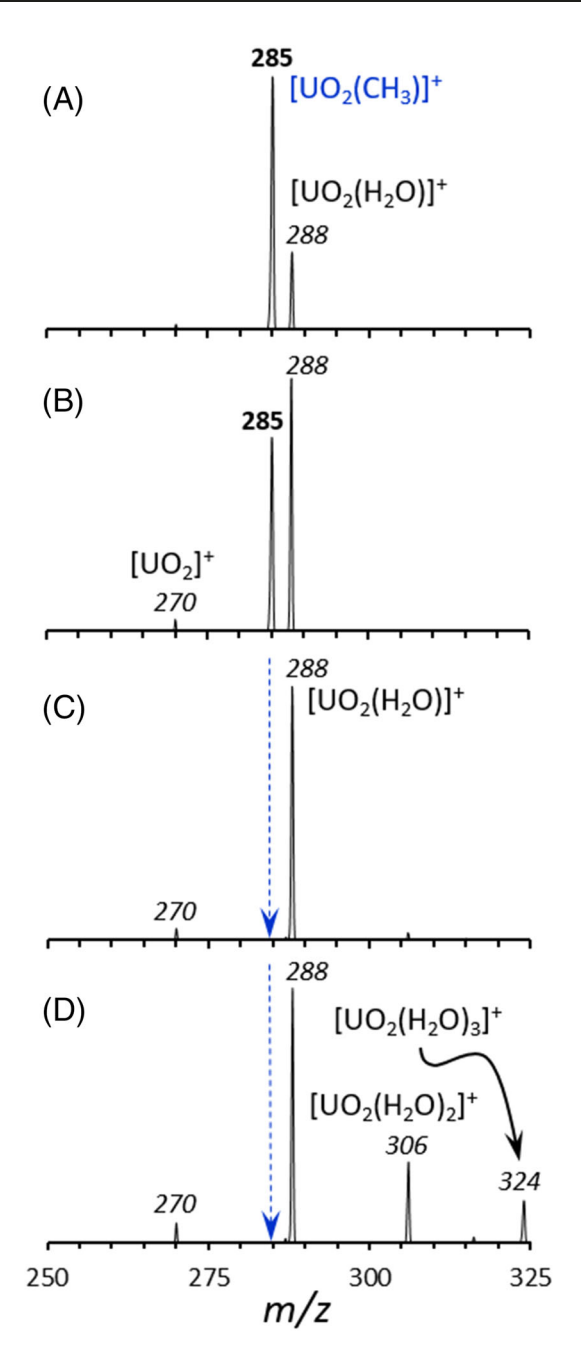


FIGURE 1 Product ion spectra generated by isolation and storage of $[UO_2(CH_3)]^+$ (m/z 285) for reaction with background H_2O : (A) 1 ms, (B) 10 ms, (C) 100 ms, and (D) 1 s. In each spectrum, the bold peak label indicates the precursor selected for ion-molecule reaction, while labels in italics represent the product ions as indicated in the text. The $[UO_2(CH_3)]^+$ ion was generated by multiple-stage collision-induced dissociation (CID) initiated with a $[UO_2(OCH_2CH_3)(CH_3CH_2OH)_2]^+$ precursor ion [Colour figure can be viewed at wileyonlinelibrary.com]

Because the electron affinity of a neutral can be used to assess the stability of an anion, we propose that the exclusive formation of $[UO_2(H_2O)]^+$ upon isolation of $[UO_2(CH_3)]^+$ for IMR likely reflects the low electron affinity of the methyl radical (+0.080 \pm 0.002 eV). Further discussion of potential competition between reactions 1 and 2 is provided below.

The next step was to create the positively charged complex $[UO_2(CH_2CH_3)]^+$. However, the MSⁿ CID of the uranyl-propionate complex, $[UO_2(O_2C-CH_2CH_3)(CH_3CH_2OH)_2]^+$, (data now shown) produced essentially the same results observed for the acetate-containing precursor: CH_3CH_2OH ligands were eliminated in sequential steps (MS/MS and MS³ stages, respectively), and subsequent CID of $[UO_2(O_2C-CH_2CH_3)]^+$ (MS⁴ stage) created $[UO_2(OH)]^+$ at m/z 287. The 1-propoxide complex $[UO_2(OCH_2CH_2CH_3)(CH_3CH_2CH_2OH)_2]^+$ was a prominent ion in the ESI spectrum of the uranyl-propionate solution prepared in 50:50 $H_2O:CH_3CH_2CH_2OH$. Initiating MSⁿ CID experiments with this precursor, we were able to generate $[UO_2(CH_2CH_3)]^+$ (MS⁴ stage, Figure S2).

CID of $[UO_2(CH_2CH_3)]^+$ (MS⁵ stage, Figure S4D) primarily caused elimination of CH_2CH_3 radical to leave $[UO_2]^+$ at m/z 270. Isolation of $[UO_2(CH_2CH_3)]^+$ for 1 ms to 1 s (Figure S3) to react with H_2O generated only $[UO_2(H_2O)]^+$ at m/z 288, presumably through a reaction similar to 1. Hydrolysis to generate $[UO_2(OH)]^+$ at m/z 287 was not observed. Exclusive loss of the CH_2CH_3 radical, with reduction of UO_2^{-2+} to $U^VO_2^+$, after association of the precursor complex with H_2O in an IMR is consistent with the negative electron affinity for the ethyl radical $(-0.263 \pm 0.089 \text{ eV})$, 36 which indicates an "unbound" state (unstable towards electron detachment³⁷).

We next examined the CID of the uranyl-acrylate precursor and began MSⁿ experiments with $[UO_2(O_2C-CH=CH_2)(CH_3CH_2OH)_2]^+$ at m/z 433. Our hypothesis was that the significantly higher electron affinity of the vinyl radical (+0.667 ± 0.024 eV)³⁸ compared with the ethyl radical would make formation of the vinyl carbanion by decarboxylation more favorable. As for the acetate and propionate precursors, CID of $[UO_2(O_2C-CH=CH_2)(CH_3CH_2OH)_2]^+$ caused the sequential elimination (MS/MS and MS³ stages, Figure 2A,B, respectively) of CH₃CH₂OH ligands to leave $[UO_2(O_2C-CH=CH_2)]^+$. However, unlike the acetate and propionate precursors, subsequent CID of $[UO_2(O_2C-CH=CH_2)]^+$ (MS⁴ stage, Figure 2C) caused decarboxylation (reaction 3) to leave $[UO_2(CH=CH_2)]^+$ at m/z 297, along with $[UO_2(O+D)]^+$ and $[UO_2(C+D)]^+$ and $[UO_2(C+D)]^+$

$$[UO_{2}(O_{2}C-CH=CH_{2})]^{+} \rightarrow [UO_{2}(CH=CH_{2})]^{+} + CO_{2}.$$
 (3)

CID of [UO₂(CH=CH₂)]⁺ generated UO₂⁺ by elimination of vinyl radical, ·CH=CH₂ (MS⁵ stage, Figure 2D). Isolation of [UO₂(CH=CH₂)]⁺ (MS⁵ stage, Figure 3) for reaction periods of 10 and 100 ms (Figure 3A,B, respectively) produced [UO₂(OH)]⁺ through a hydrolysis reaction similar to (2). At longer reaction times (1 and 10 s, Figure 3C,D, respectively), the mono-, di-, and tri-hydrates [UO₂(OH) (H₂O)]⁺, [UO₂(OH)(H₂O)₂]⁺, and [UO₂(OH)(H₂O)₃]⁺ were observed at m/z 305, 323, and 341, respectively. The [UO₂(H₂O)]⁺ ion, the dominant product when [UO₂(CH₃)]⁺ and [UO₂(CH₂CH₃)]⁺ were isolated and allowed to react with H₂O, was not observed for [UO₂(CH=CH₂)]⁺. This result is consistent with the relatively high electron affinity of the vinyl radical and the fact that formation of UO₂⁺ required collisional activation.

The multiple-stage CID spectra derived from the uranyl-benzoate precursor, $[UO_2(O_2C-C_6H_5)(CH_3CH_2OH)_2]^+$, are shown in Figure S4.

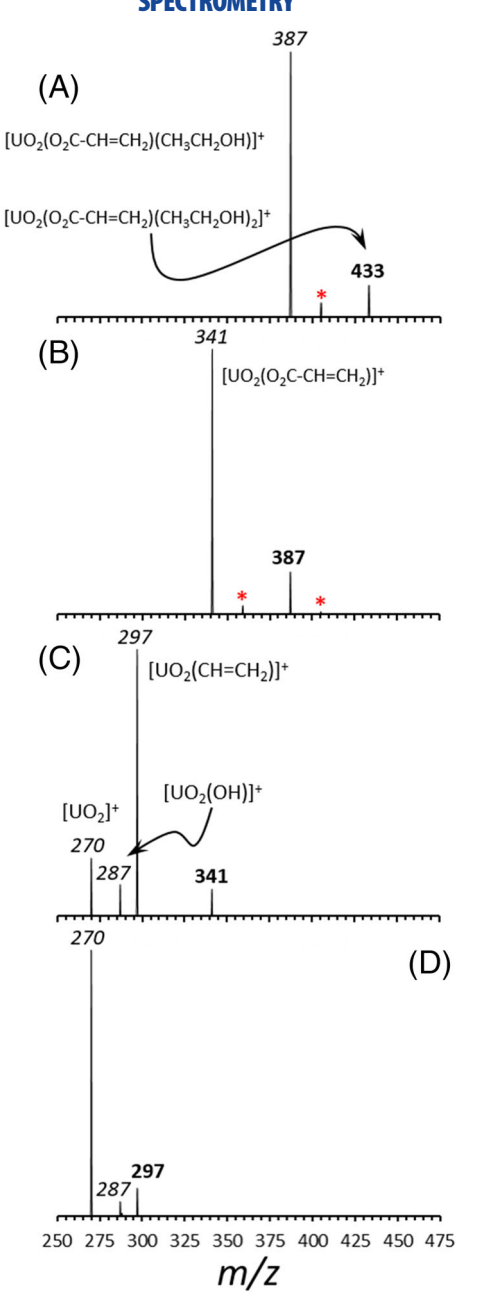


FIGURE 2 Multiple-stage collision-induced dissociation (CID) spectra derived from uranyl acrylate in 50:50 H_2O/CH_3CH_2OH : (A) CID (MS/MS) of $[UO_2(O_2C-CH=CH_2)(CH_3CH_2OH)_2]^+$ at m/z 433, (B) CID (MS³ stage) of $[UO_2(O_2C-CH=CH_2)(CH_3CH_2OH)]^+$ at m/z 387, (C) CID (MS⁴ stage) of $[UO_2(O_2C-CH=CH_2)]^+$ at m/z 341, and (D) CID (MS⁵ stage) of $[UO_2(CH=CH_2)]^+$ at m/z 297. In each CID spectrum, the bold peak label indicates the precursor selected for CID, while labels in italics identify the dissociation products. H_2O adducts are indicated with an asterisk [Colour figure can be viewed at wileyonlinelibrary. com]

CID of $[UO_2(O_2C-C_6H_5)(CH_3CH_2OH)_2]^+$ (MS/MS stage, Figure S4A) and $[UO_2(O_2C-C_6H_5)(CH_3CH_2OH)]^+$ (MS³ stage, Figure S4B) caused the elimination of single CH_3CH_2OH ligands. Subsequent CID of $[UO_2(O_2C-C_6H_5)]^+$ (MS⁴ stage, Figure S4C) at m/z 391 produced the uranyl complex with the phenyl carbanion, $[UO_2(C_6H_5)]^+$ by decarboxylation, and $[UO_2]^+$ by elimination of $C_6H_5CO_2$ radical. CID of

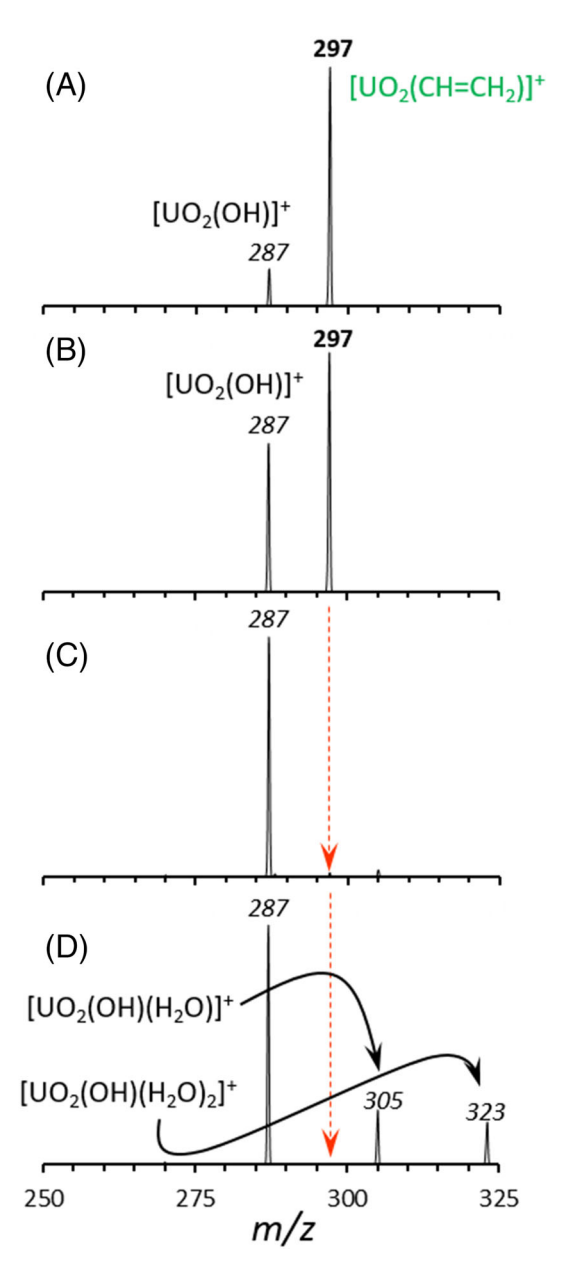


FIGURE 3 Product ion spectra generated by isolation and storage of $[UO_2(CH=CH_2)]^+$ (m/z 297) for reaction with background H_2O : (A) 10 ms, (B) 100 ms, (C) 1 s, and (D) 10 s. In each spectrum, the bold peak label indicates the precursor selected for ion-molecule reaction, while labels in italics represent the product ions as indicated in the text [Colour figure can be viewed at wileyonlinelibrary.com]

 $[\mathsf{UO}_2(\mathsf{C}_6\mathsf{H}_5)]^+$ (MS 5 stage, Figure S4D) generated UO_2^+ at $\mathit{m/z}$ 270 by elimination of the phenyl radical. Isolation of $[\mathsf{UO}_2(\mathsf{C}_6\mathsf{H}_5)]^+$ (MS 5 stage, Figure 4) for reaction periods of 10 ms to 10 s produced only $[\mathsf{UO}_2(\mathsf{OH})]^+$ by hydrolysis and the hydrates $[\mathsf{UO}_2(\mathsf{OH})(\mathsf{H}_2\mathsf{O})]^+$, $[\mathsf{UO}_2(\mathsf{OH})(\mathsf{H}_2\mathsf{O})_2]^+$ and $[\mathsf{UO}_2(\mathsf{OH})(\mathsf{H}_2\mathsf{O})_3]^+$ by subsequent $\mathsf{H}_2\mathsf{O}$ addition. The $[\mathsf{UO}_2(\mathsf{H}_2\mathsf{O})]^+$ product was not observed following isolation of $[\mathsf{UO}_2(\mathsf{C}_6\mathsf{H}_5)]^+$ to react with $\mathsf{H}_2\mathsf{O}$, consistent with the electron affinity of the phenyl radical (+1.0860 \pm .0060 eV), 39 which is higher than those of both the methyl and vinyl radicals.

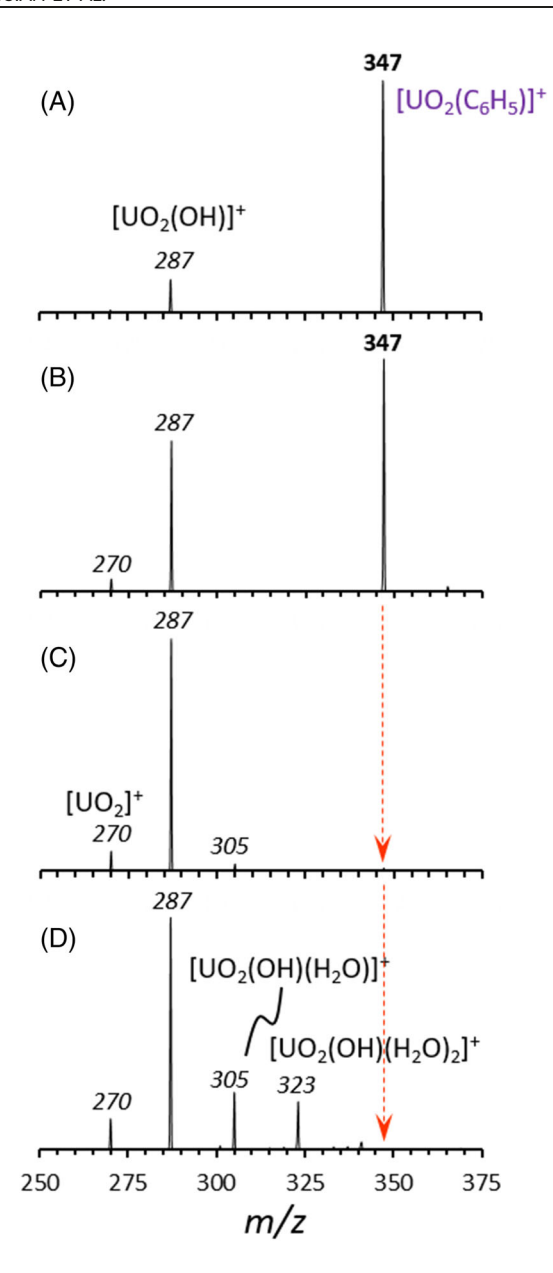


FIGURE 4 Product ion spectra generated by isolation and storage of $[UO_2(C_6H_5)]^+$ (m/z 347) for reaction with background H_2O : (A) 10 ms, (B) 100 ms, (C) 1 s, and (D) 10 s. In each spectrum, the bold peak label indicates the precursor selected for ion-molecule reaction, while labels in italics represent the product ions as indicated in the text [Colour figure can be viewed at wileyonlinelibrary.com]

3.2 | DFT calculations of reaction energies

The appearance of either $[UO_2(H_2O)]^+$ or $[UO_2(OH)]^+$ as reaction products, as described above, implicates collisions with gas-phase H_2O in the LIT. Given the different reactivity displayed by $[UO_2(CH_3)]^+$ and $[UO_2(CH_2CH_3)]^+$ on the one hand and $[UO_2(CH=CH_2)]^+$ and $[UO_2(C_6H_5)]^+$ on the other, we used density functional theory (DFT) to compute zero-point corrected relative electronic energy and reaction free energy changes for reactions 1 and 2. Computed Gibbs free energies (298 K) for reactions 1 and 2 are provided in Table 1 along with the experimentally measured branching

ratios. The zero-point corrected electronic energies for the same reactions are provided in Table S1.

Regardless of the precursor organo-uranyl species investigated, the relative change in corrected electronic energy and free energy for hydrolysis (reaction 2) is significantly more negative than for loss of a neutral radical to generate $[UO_2(H_2O)]^+$ (reaction 1). Therefore, the computed energy changes are in agreement with the reactivity measured for $[UO_2(CH=CH_2)]^+$ and $[UO_2(C_6H_5)]^+$ but not with our results for $[UO_2(CH_3)]^+$ and $[UO_2(CH_2CH_3)]^+$, which both generate $[UO_2(H_2O)]^+$ when exposed to gas-phase H_2O . This led to us to determine the extent to which the transition state energy for proton transfer, necessary to create $[UO_2(OH)]^+$ and neutral CH_4 , CH_3 — CH_3 , etc, may influence the competition between reactions 1 and 2.

Structures for the respective minima and transition states for reactions 1 and 2, using species on the reaction coordinate for $[UO_2(CH_3)]^+$ as representative examples, are provided in Figure 5. Computed structures for the remaining species are provided in

TABLE 1 Computed free energies and branching ratios for the reaction of $[UO_2(CH_3)]^+$, $[UO_2(CH_2CH_3)]^+$, $[UO_2(CH=CH_2)]^+$, and $[UO_2(C_6H_5)]^+$ with H_2O

$[UU_2(C_6H_5)]$ with H_2U										
	ΔG, kJ/mol, B3LYP									
Reaction	CH ₃	CH ₂ CH ₃	CH=CH ₂	C ₆ H ₅						
$\begin{split} [UO_2(R)]^+ + H_2O &\to [UO_2(H_2O)]^+ \\ &+ \cdot R \end{split}$	-73.6	-54.4	-24.7	-4.2						
$\begin{split} [UO_2(R)]^+ + H_2O &\to [UO_2(OH)]^+ \\ + HR \end{split}$	-167.4	-131.8	-145.9	-134.3						
	ΔG, kJ/mol, M06-L									
Reaction	CH ₃	CH ₂ CH ₃	CH ₂ CH ₃ CH=CH ₂							
$\begin{aligned} [UO_2(R)]^+ + H_2O &\rightarrow [UO_2(H_2O)]^+ \\ + \cdot R \end{aligned}$	-55.5	-29.8	-2.7	9.4						
$\begin{split} [UO_2(R)]^+ + H_2O &\to [UO_2(OH)]^+ \\ + HR \end{split}$	-177.4	-122.9	-135.4	-128.3						
	ΔG, kJ/mol, M06-2X									
Reaction	CH ₃	CH ₂ CH ₃	CH=CH ₂	C ₆ H ₅						
$\begin{aligned} [UO_2(R)]^+ + H_2O &\to [UO_2(H_2O)]^+ \\ + \cdot R \end{aligned}$	-53.0	-27.8	1.0	10.2						
$\begin{aligned} [UO_2(R)]^+ + H_2O &\rightarrow [UO_2(OH)]^+ \\ + HR \end{aligned}$	-157.5	-116.2	-128.8	-128.0						
	ΔG, kJ/mol, PBE0									
Reaction	CH ₃	CH ₂ CH ₃	CH=CH ₂	C ₆ H ₅						
$\begin{aligned} [UO_2(R)]^+ + H_2O &\to [UO_2(H_2O)]^+ \\ + \cdot R \end{aligned}$	-68.5	-40.3	-12.6	1.6						
$\begin{aligned} [UO_2(R)]^+ + H_2O &\rightarrow [UO_2(OH)]^+ \\ + HR \end{aligned}$	-168.9	-116.6	-136.3	-130.9						
	Percentage of product yield									
Reaction	CH ₃	CH ₂ CH ₃	CH=CH	C ₆ H ₅						
$\begin{aligned} [UO_2(R)]^+ + H_2O &\rightarrow [UO_2(H_2O)]^+ \\ \cdot R \end{aligned}$	+ 100.0	0 100.0	0.0	0.0						
$[UO_2(R)]^+ + H_2O \rightarrow [UO_2(OH)]^+ + HR$	+ 0.0	0.0	100.0	100.0						

Figures S5 to S7. Electronic energies (EE), zero-point energy-corrected EEs, and the sum of electron and thermal free energies are provided in Tables S2 to S5. We note here that one consideration when surveying potential minima and transition structures was that the [UO₂(H₂O)]⁺ species might isomerize to generate the dihydroxide [U(O)(OH)₂]⁺ through a proton transfer step (Scheme 1). This specific reaction was investigated for ThO₂, PaO₂⁺, UO₂²⁺, and UO₂⁺ in detail by Vasiliu et al⁴⁰ using coupled-cluster method calculations. In their study, it was determined that the "physisorbed" H₂O adduct ([UO₂(H₂O)]⁺) is approximately 50 kJ/mol more stable than the "chemisorbed" species ([U(O) (OH)₂]⁺). Moreover, the transition state energy for proton transfer to create the dihydroxide was computed to lie only 5.43 kJ/mol below the reactant energy asymptote, and the computed reaction energetics were in good agreement with experimental investigations of the rates of axial oxo ligand exchange for the species. 41,42 Because isomerization appears to be energetically unfavorable for $[UO_2(H_2O)]^+$, we neglected the energetics of this step and based our evaluation of the reactivity of the organometallic species, $[UO_2(R)]^+$, on formation either of $[UO_2(H_2O)]^+$ or $[UO_2(OH)]^+$ by reaction with H_2O .

Reaction energy diagrams for generation of $[UO_2(H_2O)]^+$ and $[UO_2(OH)]^+$ from $[UO_2(R)]^+$ computed using the M06-L functional are shown in Figure 6. The diagrams constructed from structures computed with the B3LYP, M06-2X, and PBE0 functionals are provided in Figures S8 to S10. Relative free energies for the minima and transition state structures for all species are provided in Table 2.

Referring to the structures provided in Figure 5, association of H_2O with $[UO_2(CH_3)]^+$ (structure I) creates the hydrate II. Direct elimination of CH_3 radical from II leaves $[UO_2(H_2O)]^+$ (structure III). The ion-molecule complex IV, created by intracomplex proton transfer, is created from II through the transition state structure TS II \rightarrow IV. Elimination of CH_4 leaves $[UO_2(OH)]^+$ (structure V).

As shown in the reaction energy diagram in Figure 6A, addition of H_2O to $[UO_2(CH_3)]^+$ and $[UO_2(CH_2CH_3)]^+$ to create structure II is computed to be exergonic by approximately 107 and 101 kJ/mol, respectively. The computed energies for generation of $[UO_2(H_2O)]^+$ (structure III) by elimination of CH_3 or CH_2CH_3 radical from the respective hydrates lie 55.5 and 30 kJ/mol below the entrance asymptote and 51.5 and 71 kJ/mol above the energy of structure II, respec-

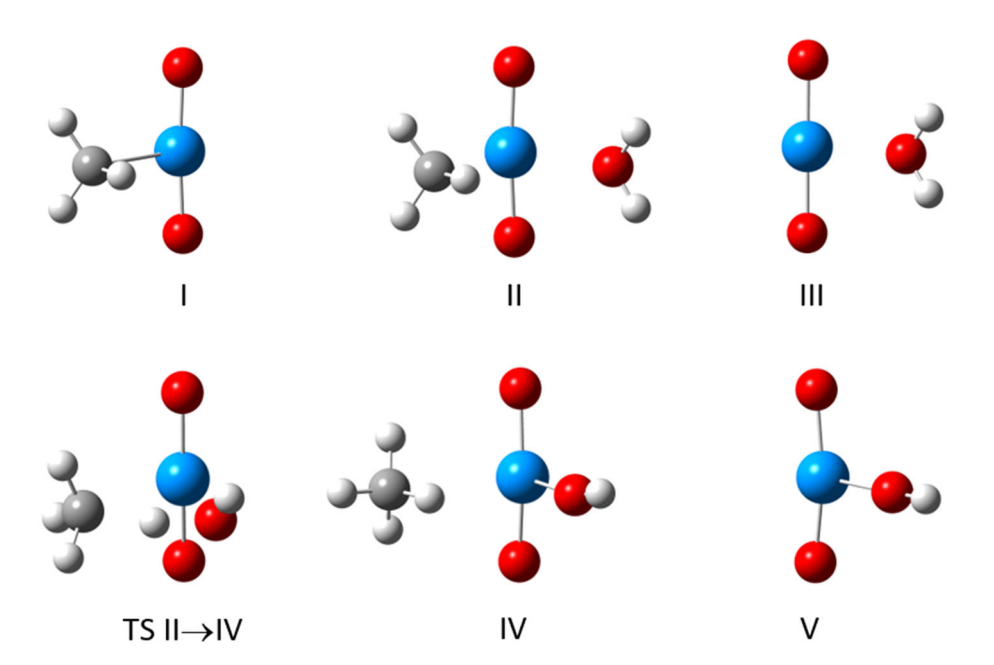


FIGURE 5 Computed structures for minima and transition state for reactions 1 and 2 in the text, using species on the reaction coordinate for $[UO_2(CH_3)]^+$ as a representative example [Colour figure can be viewed at wileyonlinelibrary.com]

SCHEME 1 Isomerization of $[UO_2(H_2O)^+]$ to create $[UO(OH)_2]^+$

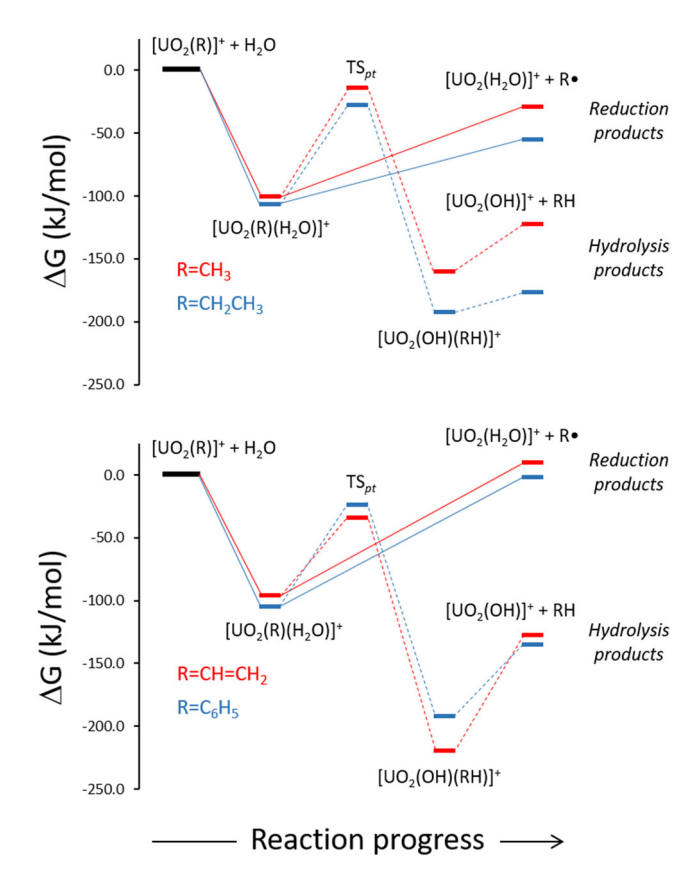


FIGURE 6 Reaction energy diagrams for (A) reaction of $[UO_2(CH_3)]^+$ and $[UO_2(CH_2CH_3)]^+$ and $[UO_2(CH=CH_2)]^+$ and $[UO_2(C_6H_5)]^+$ with H_2O . Relative free energies were calculated using data at the M06-L/SDD/6-311 + G(d,p) level of theory [Colour figure can be viewed at wileyonlinelibrary.com]

tively. For both precursor ions, the computed energy for the proton-transfer transition state (**TSII** \rightarrow **IV**) lies below the reactant asymptote, 78 and 87 kJ/mol above the hydrate structures (**II**), and (more importantly) 26.5 and 15.5 kJ/mol *above* the energy required to eject either the CH₃ or CH₂CH₃ radical to leave [UO₂(H₂O)]⁺ (structure **III**), respectively.

For $[UO_2(CH=CH_2)]^+$ and $[UO_2(C_6H_5)]^+$ (Figure 6B), the calculations predict that reaction with H_2O is also exergonic by 105.5 and 96.1 kJ/mol, respectively. However, for these two precursors, the

proton transfer transition state energy lies approximately 81 and 61 kJ/mol above the energy of the hydrate (structure II) but 21.5 and 44.1 kJ/mol *below* the energies required for direct elimination of the respective radicals to generate $[UO_2(H_2O)]^+$ (structure III). We note also that the relative energy to generate $[UO_2(H_2O)]^+$ by elimination of CH=CH₂ or C₆H₅ radical is comparable or slightly higher than the entrance channel (-2.7 and 9.4 kJ/mol for CH=CH₂ and C₆H₅ radical, respectively), which likely reflects the significantly higher electron affinities compared with those of the CH₃ and CH₂CH₃ radicals.

While our intent was not to try to determine absolute reaction thermochemistry for the respective organouranyl ions, the trends in computed energies support are consistent with experimental observations (ie, ejection of neutral radicals versus hydrolysis during reaction with $\rm H_2O$) and, in particular, support the hypothesis that the transition state energy for proton transfer influences the competition between the two pathways. We note that similar trends were observed when using the B3LYP, PBEO, and M06-2X functionals (Figures S8 to S10), thus leading to confidence in the match between theory and experiment for these species.

4 | CONCLUSIONS

To summarize, the goals of the present study were (a) to create positively charged organo-uranyl complexes with general formula $[UO_2(R)]^+$ (eg, R=CH₃, CH₂CH₃, etc.) by decarboxylation of [UO₂(O₂C-R)]⁺ precursors and (b) to identify the pathways by which the complexes, if formed, dissociate by collisional activation or otherwise react when exposed to gas-phase H2O. CID of both $[UO_2(O_2C-CH_3)]^+$ and $[UO_2(O_2C-CH_2CH_3)]^+$ causes H⁺ transfer and elimination of a ketene to leave [UO₂(OH)]⁺. However, CID of the alkoxide species [UO₂(OCH₂CH₃)]⁺ and [UO₂(OCH₂CH₂CH₃)]⁺ produced [UO₂(CH₃)]⁺ and [UO₂(CH₂CH₃)]⁺, respectively. Isolation of [UO₂(CH₃)]⁺ and [UO₂(CH₂CH₃)]⁺ for reaction with H₂O caused formation of [UO₂(H₂O)]⁺ by elimination of ·CH₂ and ·CH₂CH₃: Hydrolysis was not observed. CID of the acrylate and benzoate versions of the complexes, $[UO_2(O_2C-CH=CH_2)]^+$ and $[UO_2(O_2C-C_6H_5)]^+$, caused decarboxylation to leave [UO₂(CH=CH₂)]⁺ and [UO₂(C₆H₅)]⁺, respectively. These organometallic species react with H2O to produce

TABLE 2 Relative computed Gibbs free energies for minima I, II, III, IV, V, and for TSII \rightarrow IV, calculated relative to sum of reactant species energies (structure I + H₂O)

	ΔG, R=	CH ₃			ΔG, R=CH ₂ CH ₃			ΔG, R=CH=CH ₂			ΔG , R=C ₆ H ₅					
	M06-L	B3LYP	M06- 2X	PBE0	M06-L	B3LYP	M06- 2X	PBE0	M06-L	B3LYP	M06- 2X	PBE0	M06-L	B3LYP	M06- 2X	PBE0
I	0.0	0.0	0.0	0.0	0.0	0.0	0.0	0.0	0.0	0.0	0.0	0.0	0.0	0.0	0.0	0.0
II	-107.4	-111.3	-131.6	-115.1	-100.8	-101.4	-121.7	-105.4	-105.5	-106.8	-129.8	-111.0	-96.1	-143.4	-122.6	-104.0
III	-55.5	-73.6	-53.0	-65.8	-29.8	-54.4	-27.8	-40.3	-2.7	-24.7	1.0	-12.6	9.4	-13.2	10.2	1.6
$\begin{array}{c} \text{TS II} \rightarrow \\ \text{IV} \end{array}$	-28.5	-22.5	-42.9	-37.4	-14.3	-3.9	-26.2	-20.9	-24.2	-27.8	-39.7	-37.1	-34.7	-69.9	-55.0	-47.0
IV	-193.2	-184.8	-193.3	-181.3	-160.8	-152.0	-158.2	-147.4	-192.6	-198.9	-205.3	-196.5	-220.2	-233.4	-250.9	-224.3
V	-177.4	-167.4	-157.5	-168.9	-122.9	-131.8	-116.2	-116.6	-135.4	-145.9	-128.8	-136.3	-128.3	-138.9	-128.0	-130.9

 $[UO_2(OH)]^+$, and loss of the respective radicals to leave $[UO_2(H_2O)]^+$ was not detected. DFT calculations suggest that the $[UO_2(OH)]^+$ product is energetically favored over the hydrated $[UO_2]^+$ cation, regardless of the precursor species. However, for the $[UO_2(CH_3)]^+$ and $[UO_2(CH_2CH_3)]^+$ precursors, the transition state energy for proton transfer to generate $[UO_2(OH)]^+$ and the associated neutral alkanes is higher than the path involving direct elimination of the organic neutral to form $[UO_2(H_2O)]^+$. The situation is reversed for the $[UO_2(CH=CH_2)]^+$ and $[UO_2(C_6H_5)]^+$ precursors: The transition state for proton transfer is lower than the energy required for creation of $[UO_2(H_2O)]^+$ and elimination of $C=CH_2$ or C_6H_5 radical.

ACKNOWLEDGEMENTS

M.V.S. acknowledges support for this work in the form of start-up funds from the Bayer School of Natural and Environmental Sciences (BSNES) and Duquesne University. Laboratory space renovation was made possible with support from the National Science Foundation through grant CHE-0963450. Quantum mechanical calculations were performed using the resources of the Duquesne University Center for Computational Studies and the National Science Foundation (CHE-1726824). A.B. and A.I. acknowledge BSNES, Duquesne University, and the National Science Foundation (CHE-1659823) for support of their summer undergraduate research. This work was also supported in part by the Robert Dean Loughney Faculty Development Endowment of Duquesne University.

ORCID

Michael Van Stipdonk https://orcid.org/0000-0002-7100-4370

REFERENCES

- Van Stipdonk MJ, del Carmen Michelini M, Plaviak A, Martin D, Gibson JK. Formation of bare UO₂²⁺ and NUO⁺ by fragmentation of gas-phase uranyl-acetonitrile complexes. J Phys Chem A. 2014;118(36): 7838-7846.
- Van Stipdonk MJ, O'Malley C, Plaviak A, et al. Dissociation of gasphase, doubly-charged uranyl-acetone complexes by collisional activation and infrared photodissociation. Int J Mass Spectrom. 2016;396:22-34.
- Perez E, Hanley C, Koehler S, Pestok J, Polonsky N, Van Stipdonk M. Gas phase reactions of ions derived from anionic uranyl formate and uranyl acetate complexes. J Am Soc Mass Spectrom. 2016;27(12):1989-1998.
- 4. Van Stipdonk MJ, Hanley C, Perez E, Pestok J, Mihm P, Corcovilos TA. Collision-induced dissociation of uranyl-methoxide and uranylethoxide cations: formation of UO₂H⁺ and uranyl-alkyl product ions. *Rapid Commun Mass Spectrom*. 2016;30(16):1879-1890.
- Van Stipdonk M, Bubas A, Tatosian I, et al. Formation of [U^VOF₄]⁻ by collision-induced dissociation of a [U^{VI}O₂(O₂)(O₂C—CF₃)₂]⁻ precursor. Int J Mass Spectrom. 2018;424:58-64.
- Van Stipdonk MJ, Iacovino A, Tatosian I. Influence of background H₂O on the collision-induced dissociation products generated from [UO₂NO₃]⁺. J Am Soc Mass Spectrom. 2018;29(7):1416-1424.
- 7. Tatosian IJ, Iacovino AC, Van Stipdonk MJ. CID of $[U^{VI}O_2(CIO_4)]^+$ revisited: production of $[U^{VI}O_2(CI)]^+$ and subsequent hydrolysis to

- create $[U^{VI}O_2(OH)]^+$. Rapid Commun Mass Spectrom. 2018;32(13): 1085-1091.
- Van Stipdonk M, Anbalagan V, Chien W, Gresham G, Groenewold G, Hanna D. Elucidation of the collision-induced dissociation pathways of water and alcohol coordinated complexes containing the uranyl cation. J Am Soc Mass Spectrom. 2003:14(11):1205-1214.
- Van Stipdonk MJ, Chien W, Anbalagan V, Bulleigh K, Hanna D, Groenewold G. Gas-phase complexes containing the uranyl ion and acetone. J Phys Chem A. 2004;108(47):10448-10457.
- Van Stipdonk MJ, Chien W, Bulleigh K, Wu Q, Groenewold GS. Gasphase uranyl-nitrile complex ions. J Phys Chem A. 2006;110(3): 959-970
- Anbalagan V, Chien W, Gresham GL, Groenewold GS, Van Stipdonk MJ. Production and collision-induced dissociation of gas-phase, waterand alcohol-coordinated uranyl complexes containing halide or perchlorate anions. *Rapid Commun Mass Spectrom*. 2004;18(24): 3028-3034.
- Rios D, Rutkowski PX, Van Stipdonk MJ, Gibson JK. Gas-phase coordination complexes of dipositive plutonyl, PuO₂²⁺: chemical diversity across the actinyl series. *Inorg Chem.* 2011;50(11):4781-4790.
- 13. Heinemann C, Schwarz H. NUO^+ , A new species isoelectronic to the uranyl dication $UO_2^{2^+}$. Chem-Eur J. 1995;1(1):7-11.
- Luo M, Hu B, Zhang X, et al. Extractive electrospray ionizationmass spectrometry for sensitive detection of uranyl species in natural water samples. Anal Chem. 2010;82(1):282-289.
- Dau PD, Rios D, Gong Y, et al. Synthesis and hydrolysis of uranyl, neptunyl and plutonyl gas-phase complexes exhibiting discrete actinide-carbon bonds. Organometallics. 2016;35(9):1228-1240.
- Groenewold GS, Cossel KC, Gresham GL, et al. Binding of molecular O₂ to di- and tri-ligated [UO₂]⁺. J Am Chem Soc. 2006;128(9): 3075-3084.
- Bryantsev VS, Cossel KC, Diallo MS, et al. 2-Electron 3-atom bond in side-on (η²) superoxo complexes: U (IV) and U(V) dioxo monocations. J Phys Chem A. 2008;112(26):5777-5780.
- 18. Leavitt CM, Bryantsev VS, de Jong WA, et al. Addition of H_2O and O_2 to acetone and dimethylsulfoxide ligated uranyl(V) dioxocations. *J Phys Chem A*. 2009;113(11):2350-2358.
- Lucena AF, Carretas JM, Marçalo J, Michelini MC, Gong Y, Gibson JK. Gas-phase reactions of molecular oxygen with uranyl(V) anionic complexes—synthesis and characterization of new superoxides of uranyl (VI). J Phys Chem A. 2015;119(15):3628-3635.
- Becke AD. Density-functional thermochemistry. III. The role of exact exchange. J Chem Phys. 1993;98(7):5648-5652.
- Lee C, Yang W, Parr RG. Development of the Colle-Salvetti correlation-energy formula into a functional of the electron density. *Phys Rev B*. 1988;37(2):785-789.
- Stephens PJ, Devlin FJ, Chabalowski CF, Frisch MJ. Ab initio calculation of vibrational absorption and circular dichroism spectra using density functional force fields. J Phys Chem. 1994;98(45): 11623-11627.
- Perdew JP, Ernzerhof M, Burke K. Rationale for mixing exact exchange with density functional approximations. J Chem Phys. 1996;105(22):9982-9985.
- 24. Adamo C, Barone V. Toward reliable density functional methods without adjustable parameters: the PBEO model. *J Chem Phys.* 1999;110(13):6158-6170.
- 25. Zhao Y, Truhlar DG. The M06 suite of density functionals for main group thermochemistry, thermochemical kinetics, noncovalent interactions, excited states, and transition elements: two new functionals and

789

- systematic testing of four M06-class functionals and 12 other functionals. *Theor Chem Acc.* 2008;120:215-241.
- Peng C, Schlegel HB. Combining synchronous transit and quasi-Newton methods for finding transition states. *Israel J Chem*. 1993;33(4):449-454.
- 27. Frisch MJ, Trucks GW, Schlegel HB, et al., Gaussian 09, Revision A.02, Gaussian, Inc., Wallingford CT; 2016.
- O'Hair RAJ, Rijs N. Gas phase studies of the Pesci decarboxylation reaction: synthesis, structure, and unimolecular and bimolecular reactivity of organometallic ions. Acc Chem Res. 2015;48(2):329-340.
- O'Hair RAJ, Vrick AK, James PF. Gas phase synthesis and reactivity of the organomagnesates [CH₃MgL₂]⁻ (L=Cl and =O₂CH₃): from ligand effects to catalysis. J Am Chem Soc. 2004;126(38):12173-12183.
- Sraj LO, Khairallah GN, da Silva G, O'Hair RAJ. Who Wins: Pesci, Peters or Deacon? Intrinsic reactivity orders for organocuprate formation via ligand decomposition. *Organometallics*. 2012;31(5):1801-1807.
- 31. Woolley MJ, Khairallah GN, da Silva G, Donnelly PS, Yates BF, O'Hair RAJ. Role of the metal, ligand and alkyl group in the hydrolysis reactions of group 10 organometallic cations, [(L)M(R)]⁺. *Organometallics*. 2013;32(23):6931-6944.
- 32. Waters T, O'Hair RAJ, Wedd AG. Catalytic gas phase dehydration of acetic acid to ketene. *Int J Mass Spectrom*. 2003;228(2-3):599-611.
- 33. Graul ST, Squires RR. Gas-phase reactions of the methyl anion. J Am Chem Soc. 1989;111(3):892-899.
- Ellison GB, Engelking PC, Lineberger WC. An experimental determination of the geometry and electron affinity of CH₃. J Am Chem Soc. 1978:100(8):2556-2558.
- 35. Oliveira AM, Lu U-J, Lehman JH, et al. Photoelectron spectroscopy of the methide anion: electron affinities of ·CH₃ and ·CD₃ and inversion splitting of CH₃[−] and CD₃[−]. *J Am Chem Soc.* 2014;1237:12939-12945.

- 36. DePuy CH, Gronert S, Barlow SE, Bierbaum VM, Damrauer R. The gas phase acidities of the alkanes. *J Am Chem Soc.* 1989;111(6):1968-1973.
- Blanksby SJ, Bowie J. Carbanions: formation, structure and thermochemistry. In: Ebbering NM, ed. *Encyclopedia of Mass Spectrometry*. Vol.4 San Diego, CA: Elsevier; 2005:261-270.
- 38. Ervin KM, Gronert S, Barlow SE, et al. Bonds strengths of ethylene and acetylene. J Am Chem Soc. 1990;112(15):5750-5759.
- 39. Gunion RF, Gilles MK, Polak ML, Lineberger WC. Ultraviolet photoelectron spectroscopy of the phenide, benzyl, and phenoxide anions. Int J Mass Spectrom Ion Proc. 1992;117:601-620.
- 40. Vasiliu M, Peterson KA, Gibson JK, Dixon DA. Reliable potential energy surfaces for the reactions of H₂O with ThO₂, PaO₂⁺, UO₂²⁺ and UO₂⁺. J Phys Chem A. 2015;119(46):11422-11431.
- Rios D, Michelini MC, Lucena AF, Marçalo J, Gibson JK. On the origins of faster oxo exchange for uranyl(V) verus plutonyl(V). J Am Chem Soc. 2012;134(37):15488-15496.
- Lucena AF, Odoh SO, Zhao J, Marçalo J, Schrechenbach G, Gibson JK.
 Oxo-exchange of gas-phase uranyl, neptunyl, and plutonyl with water and methanol. *Inorg Chem.* 2014;53(4):2163-2170.

SUPPORTING INFORMATION

Additional supporting information may be found online in the Supporting Information section at the end of the article.

How to cite this article: Tatosian I, Bubas A, Iacovino A, Kline S, Metzler L, Van Stipdonk M. Formation and hydrolysis of gasphase [UO₂(R)]⁺: R=CH₃, CH₂CH₃, CH=CH₂, and C₆H₅. *J Mass Spectrom*. 2019;54:780 –789. https://doi.org/10.1002/jms.4430